Journal of The Electrochemical Society, **157** (1) B39-B44 (2010)
0013-4651/2010/157(1)/B39/6/$28.00 © The Electrochemical Society

Pulse Electrodepositions of PtRu on Large-Area Carbon Nanotubes for Enhancement of Methanol Electro-Oxidation

Yi-Fan Hsieh,* Yu-Chi Hsieh,* Pu-Wei Wu,,z Chen-Hong Liao,* and Yun-Min Chang***

Department of Materials Science and Engineering, National Chiao Tung University, Hsin-chu 300, Taiwan

We employed an electroless deposition technique to prepare Ni seeds uniformly on a carbon cloth, followed by carbon nanotube (CNT) formation at an elevated temperature. Subsequently, a pulse electrodeposition was used to impregnate PtRu nanoparticles on the CNT structure. Similar procedures were performed on carbon supports including Vulcan XC72R, BP2000, and carbon nanocapsules (CNCs) for comparison purposes. Diffraction patterns from an X-ray confirmed a PtRu alloyed phase. An analysis from inductively coupled plasma-mass spectrometry indicated that the PtRu composition was relatively unchanged. Images from scanning and transmission electron microscopes revealed dense CNTs throughout the carbon cloth with nanoparticulate PtRu evenly impregnated. Considerable PtRu aggregations were found on the CNCs and BP2000. We observed a significantly improved coulomb efficiency and an electrochemically active surface area for the CNT-grown carbon cloth. In both apparent current density and mass activity for methanol electro-oxidation, the CNT-grown carbon cloth revealed the largest values. We attribute the performance enhancement to the large-area CNT structure that allowed facile access of electrolytes.
 [DOI: 10.1149/1.3246002]

Manuscript submitted March 16, 2009; revised manuscript received September 14, 2009. Published November 10, 2009.

The development of direct methanol fuel cells (DMFCs) has recently received considerable attention for their potential applications in transportation and portable electronics.[1,2] Due to the CO poisoning in methanol dehydrogenation, electrocatalysts such as PtRu are used to improve the DMFCs efficiency.[3,4] Responsible mechanisms for methanol electro-oxidation, including bifunctional model and ligand effect, are proposed.[5,6] The bifunctional model involves a synergistic mechanism in which a partially oxidized surface Ru provides the oxygenated species to oxidize the poisoning intermediates to CO_2. The ligand effect describes the alteration of the electronic structure in Pt caused by nearby Ru atoms. Instead of directly deposited on an electrode structure, the PtRus are prepared as nanoparticles and impregnated on carbonaceous materials to obtain better distribution, size, and utilization rate. The conventional selection criteria for carbon supports are large surface area, reasonable electrical conductivity, and acceptable corrosion resistance.

Many types of carbonaceous materials are investigated as electrocatalyst supports.[7] For instance, extensive reports cover carbon blacks, mesoporous carbons, and nanostructured carbons with impressive results.[8-13] In particular, the nanostructured carbons demonstrate promising characteristics because their unique morphologies and shapes often lead to synergistic effects when electrocatalysts are deposited. To date, a wide variety of nanostructured carbons, such as carbon nanotubes (CNTs), carbon nanocapsules (CNCs), and carbon nanofibers, have been synthesized and evaluated for DMFCs.[14-18] Among them, CNTs have been investigated extensively as catalyst supports for DMFCs and polymer electrolyte fuel cells for both anodes and cathodes.[19-24] It is recognized that the CNTs demonstrate superb characteristics over conventional carbon blacks in surface structure, mechanical and thermal properties, electrical conductivity, and surface area. Moreover, due to their filamentous morphology, electrodes made of CNTs reveal a desirable porosity for facile access of electrolyte and gaseous reactants.[16]

Typical fabrication schemes for the CNT-based DMFC electrodes involve preparations of PtRu nanoparticles on the CNTs via a chemical route, followed by a physical transfer to a carbon cloth.[25] Because the transfer process deposits the catalyzed-CNTs exclusively on the carbon cloth surface, the resulting catalyst utilization rate is rather limited.[26] To obtain better catalyst efficiency, an alternative approach is to synthesize the CNTs directly on the carbon cloth, followed by electrodepositions of PtRu on the CNTs. This method is expected to produce significant improvements if the CNTs could be distributed uniformly throughout the carbon cloth. One embodiment of this method was demonstrated recently by Tsai et al., in which an evaporation method was employed to prepare Ni nuclei for CNT growth, followed by a potentiostatic deposition to grow PtRu on the CNTs.[27] However, we realize that because of a possible shadowing effect in the evaporation step, the CNTs were grown preferentially on the exterior surface of the carbon cloth. Therefore, further enhancement is likely if the CNTs seeding could be implanted underneath the carbon cloth.

In this work, we adopted an electroless deposition technique to prepare the Ni seeds uniformly throughout the carbon cloth, followed by CNT formation at an elevated temperature. Subsequently, a galvanostatic pulse deposition was conducted to deposit PtRu on the CNT-grown carbon cloth. Materials and electrochemical characterizations were carried out for methanol electro-oxidation studies.

Experimental

The CNTs were formed on a Teflon-free type-A carbon cloth from E-TEK pretreated by an electroless deposition of Ni as the catalytic seeds. First, the carbon cloth (2×6 cm) was washed in 5 M HNO_3 for 30 min at 60°C to render a hydrophilic surface. Next, in a sensitization step, the carbon cloth was immersed in a solution containing 0.3 wt % $SnCl_2$ and 2.5 wt % HCl for 5 min to ensure adequate adsorption of Sn^{2+}. Afterward, the sample was dipped into an activation solution containing 0.1 wt % $PdCl_2$ and 1 wt % HCl for 3 min, allowing spontaneous oxidation of Sn^{2+} to Sn^{4+} and reduction of Pd^{2+} to Pd to take place. Then, the activated carbon cloth was submerged in a Ni plating bath (approximately pH 6) consisting of $NiSO_4$ (20 g/L) and NaH_2PO_2 (27 g/L) at 75°C for 30 s. Upon completion, the sample was thoroughly rinsed with deionized water and alcohol and dried for 10 min.

Before the formation of CNTs, the Ni-decorated carbon cloth underwent a reduction treatment at 600°C for 10 min in mixed gases of H_2 and Ar. Subsequently, C_2H_4 was introduced for another 12 min for CNT synthesis. The flow rates for Ar, H_2, and C_2H_4 were 450, 50, and 25 mL/min, respectively. After the CNT formation, the net weight increment was 20 mg/cm^2. To deposit the PtRu nanoparticles by pulse electrodeposition, the CNT-grown carbon cloth was cut into three pieces 2×2 cm each and was inserted into a homemade sample holder that exhibited a circular opening of 1 cm^2 exposed to the electrolyte. Next, the sample was immersed in a 0.5 M H_2SO_4 solution for 5 min to prepare a hydrophilic surface. The galvanostatic pulse deposition of PtRu was performed by BaSyTec at 26°C with a plating bath including H_2PtCl_6 (99.9 wt %), $RuCl_3$ (99.9 w t%), $NaNO_2$ (97 wt %), and H_2SO_4 (97 wt %). Their concentrations were 0.005, 0.005, 0.05, and 0.25 M, respectively. The

* Electrochemical Society Student Member.
** Electrochemical Society Active Member.
z E-mail: ppwu@mail.nctu.edu.tw

parameters employed were current on time (T_{on}, 50 ms), current density (50 mA/cm^2), current off time (T_{off}, 100 ms), and total coulomb charge (8 C). A Pt foil (10 cm^2) was used as the counter electrode, and the distance between the working and counter electrodes was 3.5 cm. The current density and coulomb charge were based on the geometric area of the working electrode exposed to the electrolyte (1 cm^2).

Electrochemical characterizations were carried out under N_2 atmosphere at 26°C using a Solartron SI 1287 potentiostat. A three-electrode arrangement was adopted where the Pt foil (10 cm^2) and the Ag/AgCl were used as the counter and reference electrodes, respectively. The area for the working electrode was the geometric area exposed to the electrolyte (1 cm^2). To determine the electrochemically active surface area (ESA), cyclic voltammetric (CV) scans in 0.5 M H_2SO_4 were conducted for −0.2 to 0.7 V at 20 mV/s. For methanol electro-oxidation, the cyclic voltammetries were performed in a mixed solution of 0.5 M H_2SO_4 and 1 M CH_3OH for −0.2 to 0.9 V at 20 mV/s.

X-ray diffraction (XRD; Siemens D5000) with a Kα of 1.54 Å was used to identify the relevant phase of the PtRu nanoparticles. A transmission electron microscope (TEM; Philips Tecnai-20) was adopted to observe their morphologies and distributions on carbon supports. The loadings and molar ratios for the PtRu nanoparticles were determined by inductively coupled plasma-mass spectrometry (ICP-MS; SCIEX ELAN 5000). The surface area of the CNTs was obtained by careful removal of the deposits from the carbon cloth and was analyzed using the Brunauer, Emmett, and Teller method (BET) (Micromeritics Tristar 3000). The electrical resistivity of the CNT-grown carbon cloth was measured by a four-point probe (Keithley 2000).

For comparison purposes, identical PtRu electrodepositions and electrochemical analysis were performed on carbon cloths precoated with Vulcan XC72R (XC72R), BP2000, and CNCs. The preparation method entailed an ultrasonic mixing of 5 mg Nafion and 5 mL C_2H_5OH for 30 min, followed by the addition of 8 mg of carbons for another ultrasonication of 60 min. The carbon dispersion was then brush-painted on the carbon cloth (2 × 2 cm) with a resulting carbon loading in 2 mg/cm^2.

Results and Discussion

Electroless Ni deposition plays a critical role over subsequent CNT synthesis because the growth of CNTs is influenced greatly by the distribution and the size of the Ni seeds. From our observations, excess Ni seeds engendered overgrowths of CNTs that resulted in structural instability. Inadequate Ni seeds produced insufficient CNT coverage. After repeated tries, we determined the optimized parameters to prepare a suitable amount of Ni on the carbon cloth. The resulting Ni seeds contained 5 wt % of P. The 5 wt % of P was a codeposit from the electroless Ni bath because the NaH_2PO_2 was used as the reducing agent.

Figure 1 demonstrates the scanning electron microscope (SEM) images of the CNT-grown carbon cloth with selective areas enlarged for better contrast. As shown in Fig. 1a, the thickness for the sample became 500–600 μm, which was increased from the untreated carbon cloth of 350 μm. The structure was mostly intact with interwoven carbon fibers clearly visible. Figure 1b and c exhibits the formation of CNTs on the interior area. The CNTs were grown in large areas on the carbon fibers with adequate spaces in between. The diameter for the untreated carbon fiber was 10 μm. After CNT formation, its diameter increased significantly. According to Reshetenko et al.,[16] this filamentous morphology is conductive to electrolyte access that we believe could lead to better PtRu deposition.

To fairly evaluate the prospects of CNT as a catalyst support, we selected the XC72R, CNCs, and BP 2000 for PtRu electrodepositions. The XC72R and BP2000 are often used as the electrode materials with established properties.[28,29] The CNCs, synthesized by a flame combustion method, have demonstrated notable potentials.[30-32] Table I provides the results from material characterizations on the carbon supports under study. The CNTs revealed a surface area of 508 m^2/g, which was larger than those of XC72R and CNCs. In electrical resistivity, coating of carbon supports produced a reduced value compared to the untreated carbon cloth.

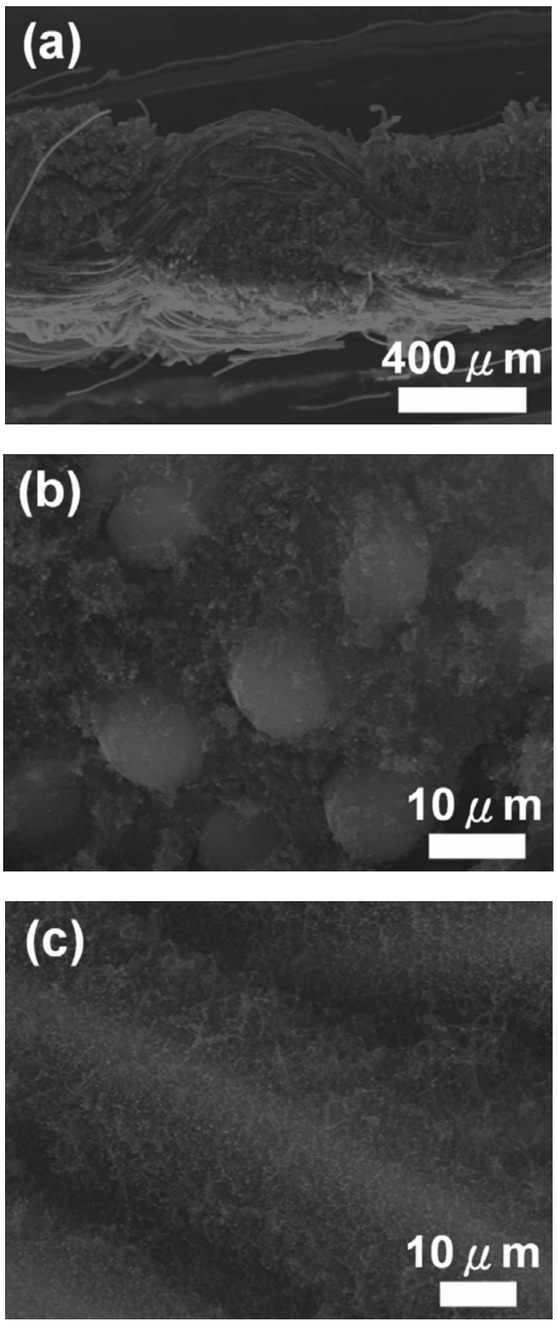

Figure 1. SEM images for the CNT-grown carbon cloth in (a) cross-sectional, (b) interior, and (c) single-fiber views.

Figure 2 presents the XRD patterns for the PtRu nanoparticles deposited on carbon cloths coated with XC72R, CNCs, BP2000, and CNTs, respectively. Due to interference from the carbon cloth and carbon supports, moderate noises in diffraction signals were evident. However, there existed several diffraction peaks, and their responsible planes were labeled accordingly. The signals from those of Pt revealed a face-centered cubic phase, with the peak positions slightly shifted to larger angles. This indicates that the Ru was alloyed in the Pt lattice because a smaller Ru atom leads to the reduc-

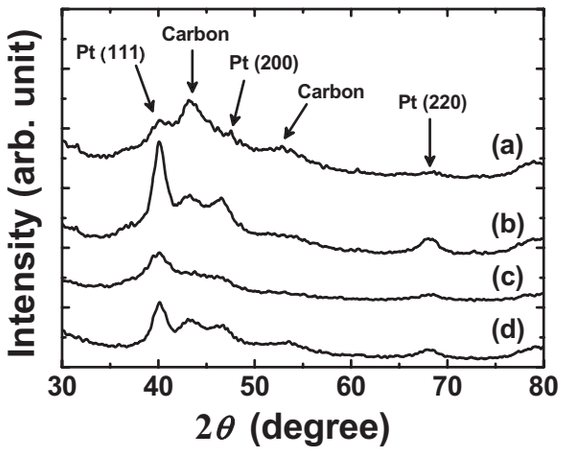

Figure 2. XRD patterns for the PtRu nanoparticles on (a) XC72R, (b) CNCs, (c) BP2000, and (d) CNTs.

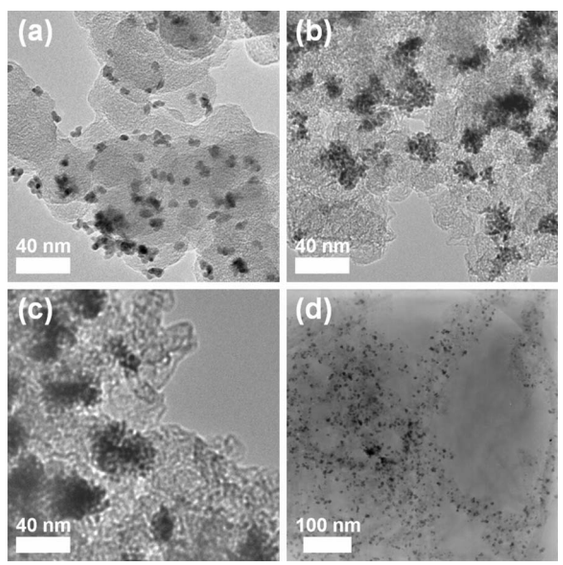

Figure 3. TEM images for the PtRu nanoparticles on (a) XC72R, (b) CNCs, (c) BP2000, and (d) CNTs.

tion of the Pt lattice. The size of the PtRu nanoparticles could be estimated by Scherrer's equation. Using the Pt(111) signals, their sizes were between 4 and 7 nm.

The TEM pictures for the PtRu nanoparticles on various carbon supports are exhibited in Fig. 3. These images were also analyzed to determine the average PtRu sizes (listed in Table I). We obtained uniform distributions of PtRu on XC72R and CNTs. In contrast, considerable aggregations were observed on the CNCs and BP2000. Because the CNCs and BP2000 consisted of relatively small carbon particles, we surmise that during electrodeposition, electrolyte transport into the micropores between these carbon particles was possibly interrupted. As a result, the formation of PtRu was confined on selective surface areas with electrolyte access. Electrolyte transport in XC72R and CNTs were not expected to be an issue because their sizes were larger, which allowed facile replenishments of Pt and Ru cations.

More details on the PtRu growth in various carbon supports can be obtained by analyzing their potential variations during galvanostatic pulse depositions. Figure 4a displays a representative potential profile of CNTs for both T_{on} and T_{off}. Apparently, both potential values exhibited a slow decline initially and became stabilized after 160 s. Potential reading at T_{on} represented the deposition voltage required for the PtRu nucleation and growth. In contrast, the potential value at T_{off} indicated the open-circuit voltage reflecting the surface state of the sample. Because the potential values fluctuated between T_{on} and T_{off}, we believe that their difference ($\Delta\eta$) is the indicator for the overpotential during PtRu depositions. Therefore, a desirable carbon support is expected to reveal a smaller overpotential and a larger coulomb efficiency. In Fig. 4b, we provide overpotential variations ($\Delta\eta$) in the CNTs and carbon supports of XC72R, CNCs, and BP2000. Clearly, the CNTs demonstrated the smallest $\Delta\eta$, while the XC72R exhibited the largest one. This suggested that the PtRu nanoparticles were relatively easier to form on the CNT-grown carbon cloth.

Variations in the PtRu molar ratios and coulomb efficiencies are shown in Fig. 5. The compositions for the PtRu nanoparticles were rather consistent, with the Pt ratio varied between 82 and 77 atom %. Pt enrichments in the PtRu were commonly encountered during electrodepositions because the redox potential of Pt was more positive than that of Ru.[33,34] The coulomb efficiency can be determined using faradaic law by taking into account the deposited PtRu weight vs the theoretic one assuming 100% conversion. The estimated efficiencies for the XC72R, CNCs, BP2000, and CNTs were 2.7, 3.7, 10.1, and 29.7%, respectively. The conventional pulse electrodeposition suffers from reduced coulomb efficiency because inherent hydrogen reduction occurs favorably on the Pt surface.[35] Therefore, those reduced coulomb efficiencies for the XC72R, CNCs, and BP2000 were not unexpected. The moderate improvement of BP2000 over those of XC72R and CNCs was attributed to its larger surface area, which provides more active sites for PtRu nucleation and growth. However, the 29.7% efficiency on the CNTs was remarkable. This value is the highest reported so far. We realize that after proper seeding of Ni, the CNT growth on the carbon cloth was uniformly distributed for both surface and interior. Sufficient spac-

Table I. Material characteristics for carbon supports and PtRu nanoparticles.

	Carbon cloth	XC72R	CNCs	BP2000	CNTs
Surface area[a]	N/A	254[b]	333	1500[c]	508
Electrical resistivity[d]	60	56	40	35	46
PtRu size[e]	N/A	6.08	4.80	4.33	4.54
PtRu size[f]	N/A	6.75	5.92	5.32	5.33

[a] Value (m^2/g) obtained in powder form via BET measurement.
[b] Value obtained from Cabot catalog.
[c] Value obtained from Cabot catalog.
[d] Value ($m\Omega$ cm) obtained on carbon cloths.
[e] Value (nm) obtained from XRD.
[f] Value (nm) obtained from TEM image.

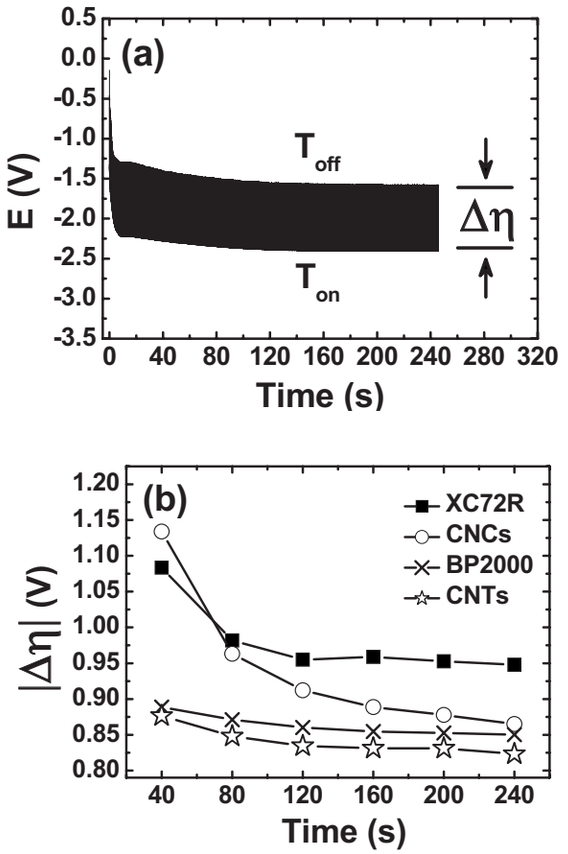

Figure 4. (a) A representative potential profile of the CNT-grown carbon cloth for both T_{on} and T_{off} during PtRu pulse depositions. (b) Overpotential variations ($\Delta\eta$) in various carbon supports.

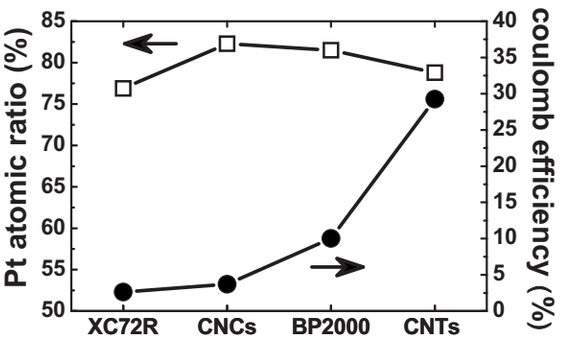

Figure 5. Variations in the Pt atomic ratio and the coulomb efficiency on various carbon supports.

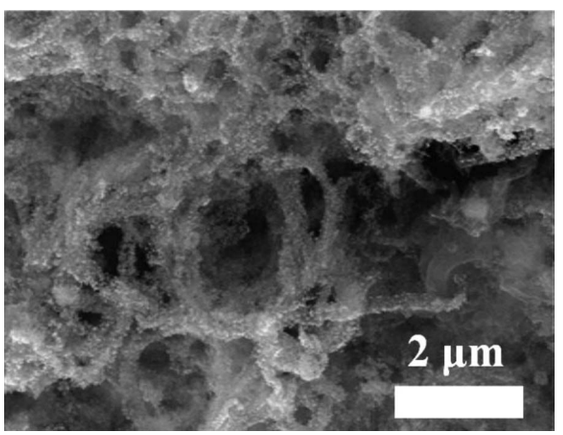

Figure 6. SEM images of the PtRu nanoparticles on the CNT-grown carbon cloth.

ing between the CNTs facilitated percolation of plating electrolyte, which favored PtRu deposition over H_2 formation. Our argument can be confirmed by the SEM images, shown in Fig. 6, for the PtRu deposited on the CNT-grown carbon cloth. An individual CNTs was impregnated with PtRu evenly. Moreover, Fig. 4b also confirmed the superiority of the CNT-grown carbon cloth for the PtRu deposition.

The determination of the catalyst loading (listed in Table II) revealed a significant difference contingent on the carbon supports. The loading on the CNTs exhibited the highest value of 1.139 mg/cm^2. In contrast, the value on the XC72R showed the lowest amount of 0.103 mg/cm^2. Except the CNTs, the PtRu loadings were proportional to the surface area of the carbon materials.

Table II. Loading of PtRu and Pt as well as electrochemical parameters from CV curves in apparent current density and mass activity of PtRu nanoparticles deposited on carbon supports.

	Loading		Forward scan			Backward scan			
	PtRu[a] (mg)	Pt[b] (mg)	V_f [c] (mV)	i_f [d] (mA/cm^2)	i_f [e] [mA/(Pt mg)]	V_b [f] (mV)	i_b [g] (mA/cm^2)	i_b [h] [mA/(Pt mg)]	ESA[i] (cm^2)
XC72R	0.103	0.089	0.54	26.3	295.1	0.46	8.9	99.9	8.6
CNCs	0.144	0.129	0.55	37.1	286.6	0.41	10.2	78.9	23.4
BP2000	0.391	0.349	0.52	73.3	209.8	0.38	5.0	14.3	176.5
CNTs	1.139	1.000	0.74	380.5	380.5	0.52	148.8	148.8	316.8

[a] Total weight of Pt and Ru as determined by ICP-MS.
[b] Weight of Pt alone as determined by ICP-MS.
[c] Peak potential in forward scan.
[d] Peak apparent current density in forward scan.
[e] Peak mass activity in forward scan.
[f] Peak potential in backward scan.
[g] Peak apparent current density in backward scan.
[h] Peak mass activity in backward scan.
[i] ESA from hydrogen adsorption.

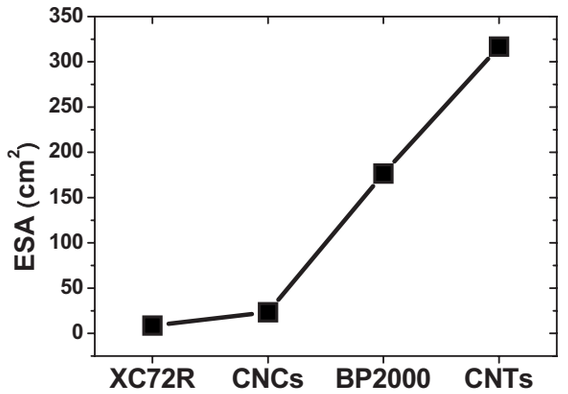

Figure 7. Variations in ESA on various carbon supports.

Because the CNTs were grown directly on the carbon cloth to form a dense three-dimensional structure, some of the CNTs might not be as accessible to the electrolyte as others. Nevertheless, the current efficiency of the CNTs was still significantly higher than those of XC72R, CNCs, and BP2000.

Figure 7 presents the ESA of PtRu on various carbon supports. These values were obtained by the integrated charge in the hydrogen adsorption region using methods established by Navessin et al. and Liu et al.[36,37] In general, the ESA is proportional to the Pt surface available for hydrogen adsorption and desorption. Hence, a larger ESA indicates a higher activity for methanol dehydrogenation. The estimated ESAs for XC72R and BP2000 were 8.57 and 176.54 cm^2, respectively. The ESA for the CNTs was 316.78 cm^2. This amounts to a 3700% improvement as opposed to XC72R. However, the PtRuloading on the CNTs was only 1100% over that of XC72R. Our ESA results suggested a significantly enhanced utilization rate of Pt on the CNT support.

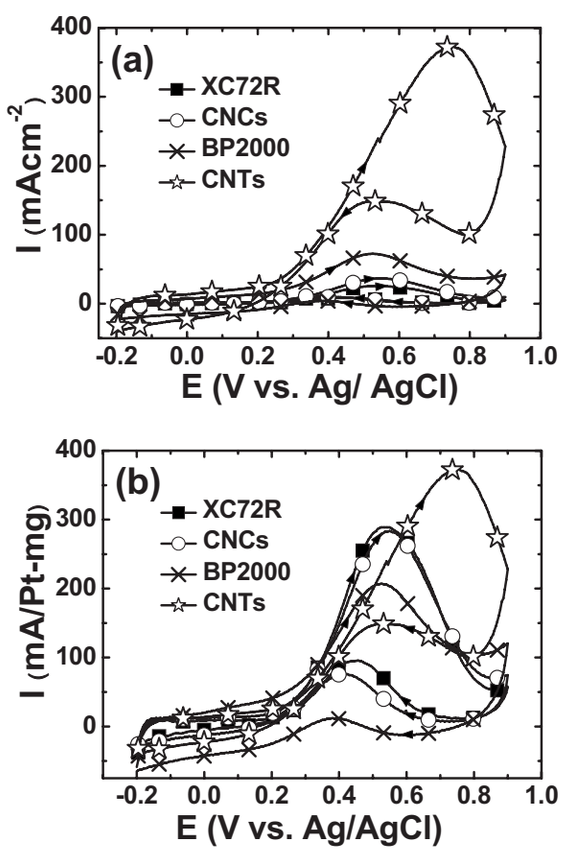

Figure 8. CV curves for the PtRu nanoparticles on various carbon supports in (a) apparent current density and (b) mass activity.

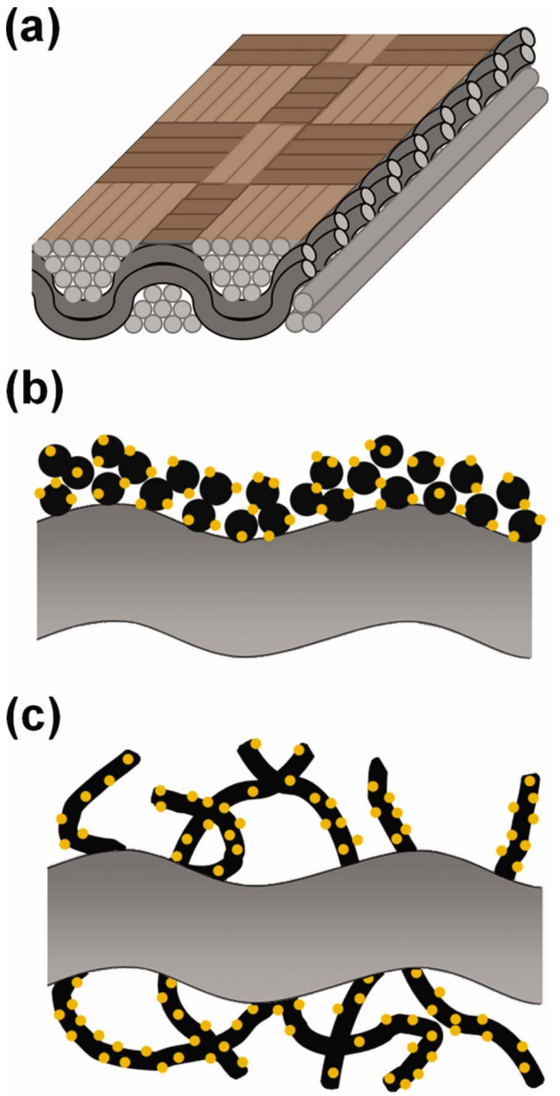

Figure 9. (Color online) A schematic diagram of (a) carbon cloth and PtRu-deposited carbon cloths from (b) physical transfer and (c) electroless routes.

Figure 8 demonstrates the CV curves on methanol electro-oxidation in apparent current densities (mA/cm^2) and mass activities (mA/mg). Clearly, current responses from forward and backward scans appeared. Relevant information, including the peak potentials, peak current densities, and peak mass activities, are listed in Table II. As shown in Fig. 8a, the order in apparent current density was CNTs, BP2000, CNCs, and XC72R. This sequence agreed well with that of ESA, indicating that a larger ESA contributed to a higher catalytic activity. Moreover, the peak potentials in forward scans shift slightly to higher values with increasing ESA. Figure 8b exhibits the profiles for mass activities. Similarly, the order for mass activities followed what was observed in apparent currents; CNTs, BP2000, CNCs, and XC72R. The results indicated that the growth of CNTs was conductive to effective use of catalyst particles.

Figure 9 provides a schematic diagram to illustrate the underlying rationale for the moderate mass activity improvement from the PtRu nanoparticles on the CNTs compared to those of XC72R,

CNCs, and BP2000. In the CNT scenario, an electroless-derived Ni seeding ensures the growth of large-area CNTs throughout the carbon cloth with sufficient space in between. This allows for desirable electrolyte percolation that not only facilitates better PtRu electrodepositions but also promotes a larger catalytic activity for methanol electro-oxidation. In contrast, for the remaining carbon supports, the PtRu nanoparticles were deposited mostly on the carbon surface because of the physical transfer involved. Hence, a reduced ESA and catalyst utilization rate were expected. Our results confirmed the advantage of using an electroless deposition approach to prepare proper Ni seeding for a large-area CNT growth. With a desirable CNT formation, a significant enhancement for methanol electro-oxidation can be obtained.

Conclusion

Large-area CNTs were formed throughout the carbon cloth pretreated with electroless-derived Ni seeds. Subsequently, a pulse electrodeposition was employed to fabricate PtRu nanoparticles on the CNT structure. Similar procedures were carried out on XC72R, CNCs, and BP2000. SEM and TEM images indicated that the growth of CNTs took place uniformly with PtRu evenly impregnated. In contrast, considerable PtRu aggregations were found on the CNCs and BP2000. The composition of PtRu was relatively unchanged among these samples. However, we observed significantly improved coulomb efficiency, PtRu loading, and ESA on the CNT-grown carbon cloth. In both apparent current density and mass activity for methanol electro-oxidation, the CNT-grown carbon cloth revealed the largest values. The observed enhancement was attributed to the desirable CNT structure that allowed facile access of electrolyte.

Acknowledgments

The authors are grateful to Professor Pang Lin and Professor George Tu for their kind assistance with the laboratory equipment.

National Chiao Tung University assisted in meeting the publication costs of this article.

References

1. C. S. Karthikeyan, S. P. Nunes, L. A. S. A. Prado, M. L. Ponce, H. Silva, B. Ruffmann, and K. Schulte, *J. Membr. Sci.*, **254**, 139 (2005).
2. F. Liu, G. Lu, and C. Y. Wang, *J. Electrochem. Soc.*, **153**, A543 (2006).
3. E. Christoffersen, P. Liu, A. Ruban, H. L. Skriver, and J. K. Norskov, *J. Catal.*, **199**, 123 (2001).
4. D. C. Papageorgopoulos and F. A. de Bruijn, *J. Electrochem. Soc.*, **149**, A140 (2002).
5. W. Zhou, Z. Zhou, S. Song, W. Li, G. Sun, P. Tsiakaras, and Q. Xin, *Appl. Catal., B*, **46**, 273 (2003).
6. F. Vigier, C. Coutanceau, F. Hahn, E. M. Belgsir, and C. Lamy, *J. Electroanal. Chem.*, **563**, 81 (2004).
7. H. Liu, C. Song, L. Zhang, J. Zhang, H. Wang, and D. P. Wilkinson, *J. Power Sources*, **155**, 95 (2006).
8. A. S. Aricò, S. Srinivasan, and V. Antonucci, *Fuel Cells*, **1**, 133 (2001).
9. Y. Takasu, T. Kawaguchi, W. Sugimoto, and Y. Murakami, *Electrochim. Acta*, **48**, 3861 (2003).
10. K. Y. Chan, J. Ding, J. Ren, S. Cheng, and K. Y. Tsang, *Mater. Chem.*, **14**, 505 (2004).
11. G. S. Chai, S. B. Yoon, J. H. Kim, and J. S. Yu, *Chem. Commun. (Cambridge)*, **2004**, 2766 (2004).
12. C. A. Bessel, K. Laubernds, N. M. Rodriguez, and R. T. K. Baker, *J. Phys. Chem. B*, **105**, 1115 (2001).
13. T. Hyeon, S. Han, Y. E. Sung, K. W. Park, and Y. W. Kim, *Angew. Chem., Int. Ed.*, **42**, 4352 (2003).
14. S. S. Dipti, U. C. Chung, J. P. Kim, and W. S. Chung, *Phys. Status Soidi A*, **204**, 4174 (2007).
15. K. Vinodgopal, M. Haria, D. Meisel, and P. Kamat, *Nano Lett.*, **4**, 415 (2004).
16. T. V. Reshetenko, H. T. Kim, and H. J. Kweon, *Electrochim. Acta*, **53**, 3043 (2008).
17. Y. M. Lin, Y. M. Chang, P. W. Wu, P. Lin, Y. Y. Li, C. Y. Wu, C. F. Tsai, and K. Y. Yeh, *J. Appl. Electrochem.*, **38**, 507 (2008).
18. M. Okada, Y. Konta, and N. Nakagawa, *J. Power Sources*, **185**, 711 (2008).
19. Y. Lin, X. Cui, C. Yen, and C. M. Wai, *J. Phys. Chem. B*, **109**, 14410 (2005).
20. S. Takenaka, H. Matsumori, H. Matsune, E. Tanabe, and M. Kishida, *J. Electrochem. Soc.*, **155**, B929 (2008).
21. X. Wang, M. Waje, and Y. Yan, *Electrochem. Solid-State Lett.*, **8**, A42 (2005).
22. K. Shimizu, I. F. Cheng, J. S. Wang, C. H. Yen, B. Yoon, and C. M. Wai, *Energy Fuels*, **22**, 2543 (2008).
23. C. Y. Du, T. S. Zhao, and Z. X. Liang, *J. Power Sources*, **176**, 9 (2008).
24. W. Li, X. Wang, Z. Chen, M. Waje, and Y. Yan, *Langmuir*, **21**, 9386 (2005).
25. C. C. Chien and K. T. Jeng, *Mater. Chem. Phys.*, **99**, 80 (2006).
26. G. Girishkumar, K. Vinodgopal, and P. V. Kamat, *J. Phys. Chem. B*, **108**, 19960 (2004).
27. M. C. Tsai, T. K. Yeh, and C. H. Tsai, *Mater. Chem. Phys.*, **109**, 422 (2008).
28. P. Sivakumar and V. Tricoli, *Electrochim. Acta*, **51**, 1235 (2006).
29. C. C. Yang, S. J. Chiu, and C. T. Lin, *J. Power Sources*, **177**, 40 (2008).
30. T. C. Liu and Y. Y. Li, *Carbon*, **44**, 2045 (2006).
31. Y. M. Chang, Y. C. Hsieh, and P. W. Wu, *Diamond Relat. Mater.*, **18**, 501 (2009).
32. C. Y. Wu, P. W. Wu, P. Lin, Y. Y. Li, and Y. M. Lin, *J. Electrochem. Soc.*, **154**, B1059 (2007).
33. A. N. Gavrilov, O. A. Petrii, A. A. Mukovnin, N. V. Smirnova, T. V. Levchenko, and G. A. Tsirlina, *Electrochim. Acta*, **52**, 2775 (2007).
34. M. C. Tsai, T. K. Yeh, Z. Y. Juang, and C. H. Tsai, *Carbon*, **45**, 383 (2007).
35. Z. D. Wei, S. G. Chen, Y. Liu, C. X. Sun, Z. G. Shao, and P. K. Shen, *J. Phys. Chem. C*, **111**, 15456 (2007).
36. T. Navessin, M. Eikerling, Q. Wang, D. Song, Z. Liu, J. Horsfall, K. V. Lovell, and S. Holdcroft, *J. Electrochem. Soc.*, **152**, A796 (2005).
37. Z. Liu, X. Y. Ling, B. Guo, L. Hong, and J. Y. Lee, *J. Power Sources*, **167**, 272 (2007).